論文 / 著書情報
Article / Book Information

Title	Automatic determination of LQR weighting matrices for active structural control
Authors	Kou Miyamoto, Jinhua She, Daiki Sato, Nobuaki Yasuo
Citation	Engineering Structures, Vol. 174, pp. 308-321
Pub. date	2018, 11
DOI	https://doi.org/10.1016/j.engstruct.2018.07.009
Creative Commons	See next page.
Note	This file is author (final) version.

License

Automatic determination of LQR weighting matrices for active structural control

Kou Miyamoto[a) b)], Jinhua She[c)], Daiki Sato[d)], Nobuaki Yasuo[e),f) *]

a) : Dept. of Architecture and Building Engineering, Tokyo Institute of Tech.
b) : Research Fellow of Japan Society for the Promotion of Science DC2
c) : Dept. of Mechanical Engineering, School of Engineering, Tokyo University of Tech.
d) : FIRST, Tokyo Institute of Technology.
e) : Dept. of Computer Science, Tokyo Institute of Technology.
f) : Research Fellow of Japan Society for the Promotion of Science DC1.

*: Corresponding author

Abstract

This paper presents a method for the automatic selection of weighting matrices for a linear-quadratic regulator (LQR) in order to design an optimal active structural control system. The weighting matrices of a control performance index, which are used to design optimal state-feedback gain, are usually determined by rule of thumb or exhaustive search approaches. To explore an easy way to select optimal parameters, this paper presents a method based on Bayesian optimization (BO). A 10-degree-of-freedom (DOF) shear building model that has passive base isolation (PBI) under the building is used as an example to explain the method. A control performance index that contains the absolute acceleration, along with the inter-story drift and velocity of each story, is chosen for the design of the controller. An objective function that contains the maximum absolute acceleration of the building is chosen for BO to produce optimal weighting matrices. In the numerical example, a restriction on the displacement of the PBI is used as a constraint for the selection of weighting matrices. First, the BO method is compared to the exhaustive search method using two parameters in the weighting matrices to illustrate the validity of the BO method. Then, thirty-three parameters (which are automatically optimized by the BO method) in the weighting matrices are used to elaborately tune the controller. The control results are compared to those for the exhaustive search method and conventional optimal control, in terms of the control performance of the relative displacement, absolute acceleration, inter-story-drift angle, and the story-shear coefficient of each story. The damping ratio for each mode, and the control energy and power are also compared. The comparison demonstrates the validity of the method.

Keywords: Active structural control (ASC), Linear-quadratic regulator (LQR), Absolute acceleration, Inter-story drift, Passive base isolation (PBI), Bayesian optimization, Gaussian process.

---

1. Introduction

Over the last a couple of decades, the number of passive-base-isolated buildings has markedly increased. In particular, such demand in Japan has been increasing significantly after the Kobe earthquake in 1995. Nowadays, passive-base isolation (PBI) is widely used in high-rise buildings to protect properties and people inside [1].

The active structural control (ASC) strategy has also been studied to yield good control performance since around 1990. This strategy is now being widely used in large-scale buildings all over the world [2].

Many methods have been proposed for the design of a control system for ASC. Among them, the linear quadratic regulator (LQR) is one of the most commonly used methods, and has been extensively investigated [3]-[16]. The LQR designs a state-feedback gain by minimizing a performance index that contains a weighted state and control input. Loh at el. conducted an experiment using a real-scale active tendon, and showed the effectiveness of the LQR for a real-scale structure [3]. Sedegh et al. compared LQR to PD/PID controllers in a high-rise building application [15]. Chu et al. also conducted an experiment for tuned-mass damper (TMD) structures considering a time delay in a control action [16].

While the state in a performance index is usually defined by a relative displacement and relative velocity, some studies chose a performance index from different viewpoints. Other definitions included elastic and kinetic energy [6, 7], absolute acceleration [10], or the inter-story drift [14]. However, Miyamoto et al. [4] and She et al. [5] applied the equivalent-input-disturbance (EID) approach to ASC. The configuration of an EID-based system contained state feedback and a state observer, and the LQR method was used to design the gains of both.

Although the LQR method is widely used, the selection of weighting matrices is largely determined by experience. The weighting matrices in the performance index are mainly determined by trial-and-error [17]. Fuji at el. considered the influence of the weighting matrices of a performance index containing only absolute acceleration for a model with a single degree of freedom (DOF) [18]. However, most buildings have multiple DOFs, and it is important to select weighting matrices for a performance index that contain other items in addition to absolute acceleration.

An exhaustive search method is computationally expensive to search for suitable weighting matrices of a state for a high-DOF model. To ease the selection of the weighting matrices, Miyamoto at el. used the same weights for both the relative displacement and velocity [4]. While this reduces

the burden for the design of a state-feedback gain, the designed gain may not meet the desired expectations. Harvey et al. presented a cheap optimal control method [19]. It calculates the weighting matrices of a state for a performance index that only contains a weighted quadratic term of the state. Kumar et al. proposed a new method for selecting LQR weighting matrices [20]. It guarantees the frequency-domain characteristics of a conventional LQR. Kawasaki et al. developed a method to select a controller based on the pole placement method [21]. Fujii et al. presented an ILQ (Inverse-LQ) method based on pole placement and the inverse problem [22]. Since methods require tuning parameters, which are damping ratio, ordinal frequency, pole and etc; an exhaustive search is needed to find appropriate parameters. Moreover, if the plant is high-DOF system, it is difficult to find these parameters.

In contrast, the Bayesian optimization (BO) method, which is a nonparametric optimization approach, can be used to select weighting matrices automatically. Even if an objective function is unknown, it can be estimated by a Gaussian process. This method has been used to select a weighting matrix in [23, 24, 25] in which the objective function was set to be the value of the performance index of the LQR. One problem is that even if the value of the performance index is small, some state responses may be very big.

In ASC for a PBI building, the suppression of both displacement and absolute acceleration is important. Note that PBI enlarges the natural period of the building. This may result in a large displacement that extends beyond the allowable range. Thus, the suppression of displacement is necessary. However, suppressing absolute acceleration not only protects the structures by reducing the story shear coefficient, it also protects people and property by preventing things such as furniture and equipment from falling over. For these reasons, optimizing a performance index that contains only the displacement or the absolute acceleration may not produce a satisfactory result. A large number of parameters must be tuned in order to design a satisfactory control system. It is desirable to find an easy way to select those parameters.

This paper uses the BO method for the automatic selection of LQR weighting matrices for ASC for the first time. A performance index containing the absolute acceleration, the inter-story drift, and the inter-story velocity of each story of a PBI building is optimized, and the displacement of the PBI story is required to be less than or equal to a prescribed value. This is used as a constraint on the optimization. The weighting matrices in the performance index are determined by optimizing an objective function for the absolute acceleration.

2. Structural model and control design

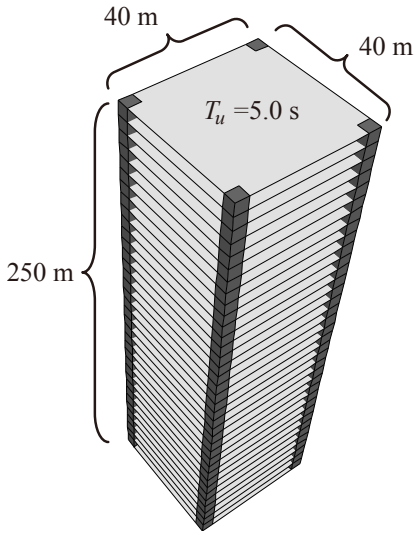

Fig. 1. Model of building

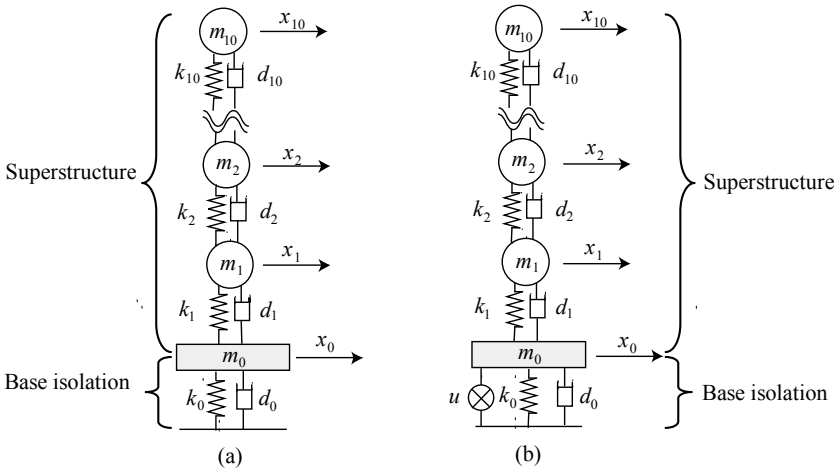

Fig. 2. 11-DOF models (a) without and (b) with an active structural control device

This section describes the structural model and the design of a state-feedback gain. This study used 10-DOF shear building model with a height of 250 m (Fig. 1) to illustrate the design methodology. A PBI is located under the structure and an ASC device is installed at the PBI story. Thus, the model of the structure is 11-DOF (10 DOFs for the superstructure and 1 DOF for the PBI) (Fig. 1). In this study, an actuator was considered as a device for ASC.

The parameters of the superstructure and the PBI are as follows:

Mass of passive base-isolation story per square meter: 2551 kg/m^2

Damping for passive base-isolation period (ζ_0)**:** 0.05

Area of superstructure：40 m x 40 m

Natural first mode period of superstructure（T_u）： 5.0 s

Density of superstructure（for all stories)： 175 kg/m^3

Height of superstructure（h_u)：= T_u/0.02 m

Each story height of superstructure（h_i)：= h_u/10

Damping of superstructure： stiffness-proportional damping model $d_i = 2\zeta_u / \omega_i k_1$ (damping ratio of the first mode: 0.02)

Stiffness of superstructure [27]： The stiffness of the *i*-th story is

$$\begin{cases} k_i = \dfrac{\omega^2 \cdot m_i \cdot \phi_i + k_{i+1}(\phi_{i+1} - \phi_i)}{\phi_i - \phi_{i-1}}, & i = 2,...,9, \\ k_1 = \dfrac{\omega^2 \cdot m_1 \cdot \phi_1 + k_2(\phi_2 - \phi_1)}{\phi_1}, & k_{10} = \dfrac{\omega^2 \cdot m_{10} \cdot \phi_{10}}{\phi_{10} - \phi_9}, \end{cases} \tag{1}$$

where ω is the first natural circular frequency; and for the *i*-th story (i = 0, 1, ..., 10), ϕ_i is the first natural mode and m_i is the mass, which is given by the product of the floor space (40 m × 40 m), the height of the *i*-th story, and the density of the superstructure. In this study, the straight-line mode was used as the first mode to design the stiffness of each story. Thus, they were selected to be $\phi_{\cdot\{1,2,...,n\}} = 1/n,\ \ 2/n,..., n/n$ for an *n*-story building.

In order to use the LQR method, which is a linear control strategy, laminated rubber in the PBI is modeled as a linear spring [Fig. 2 (a)], and the viscous damper in the PBI is modeled as a linear dashpot [Fig. 2 (b)]. The stiffness, k_0, and the damping coefficient, d_0, of the PBI are

$$k_0 = \frac{T_0^2}{4\pi^2(M_S + m_0)}, \text{ and} \tag{2}$$

$$d_0 = 2\xi_0\sqrt{(M_S + m_0)k_0}, \tag{3}$$

where T_0 is the period of the PBI if the superstructure is assumed to be a rigid body, M_S is the total mass of the superstructure, and m0 is the mass of the PBI, which is given by the product of the floor space (40 m × 40 m) and the mass of the PBI story per square meter.

The mass of the ASC device is assumed to be very small compared to the mass of the building and therefore is ignored in this study.

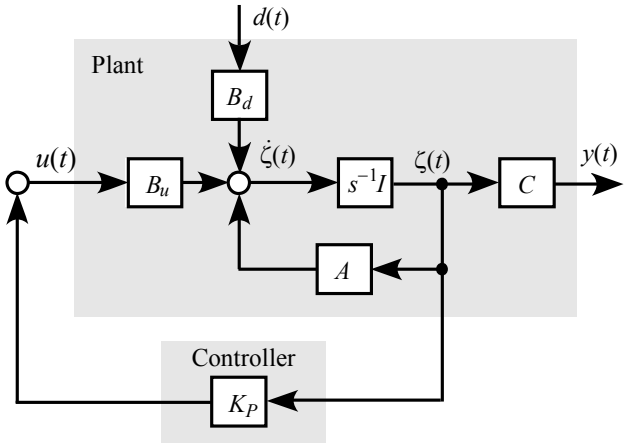

Fig. 3. Block diagram of state-feedback control system containing (5) and (7).

Remark 1: A simple shear building model was used in this study. However, if the bending, moment, and other items of a building must to be considered, then a three-dimensional model can be used to address those issues [28, 29, 30]. A performance index for a three-dimensional model was also presented in [30].

The dynamics of the structure with an active control input, $u(t)$, is described by

$$\boldsymbol{M}\ddot{\boldsymbol{x}}(t)+\boldsymbol{D}\dot{\boldsymbol{x}}(t)+\boldsymbol{K}\boldsymbol{x}(t)=-\boldsymbol{M}\boldsymbol{E}\ddot{\boldsymbol{x}}_{\boldsymbol{g}}(t)+\boldsymbol{E}_{\boldsymbol{u}}\boldsymbol{u}(t), \tag{4}$$

where $\boldsymbol{M}$ is the mass matrix, $\boldsymbol{D}$ is the damping matrix, $\boldsymbol{K}$ is the stiffness matrix, $\boldsymbol{E}$ is the disturbance input matrix, $\boldsymbol{E_u}$ is the active-control input matrix, $\boldsymbol{x}(t)$ is the displacement vector of each story, and $\ddot{x}_{\mathrm{g}}(t)$ the is acceleration of the ground. The state-space expression of (4) is

$$\begin{cases}\dot{\boldsymbol{z}}(t)=\boldsymbol{A}\boldsymbol{z}(t)+\boldsymbol{B}\boldsymbol{u}(t)+\boldsymbol{B}_{\boldsymbol{d}}\ddot{\boldsymbol{x}}_{\boldsymbol{g}}(t),\\ \boldsymbol{y}(t)=\boldsymbol{C}\boldsymbol{z}(t),\end{cases} \tag{5}$$

where

$$\begin{cases}\boldsymbol{z}(t)=\begin{bmatrix}\boldsymbol{x}(t)\\ \dot{\boldsymbol{x}}(t)\end{bmatrix},\\ \boldsymbol{A}=\begin{bmatrix}\boldsymbol{0}_{11\times 11} & \boldsymbol{I}_{11}\\ -\boldsymbol{M}^{-1}\boldsymbol{K} & -\boldsymbol{M}^{-1}\boldsymbol{D}\end{bmatrix},\quad \boldsymbol{B}=\begin{bmatrix}\boldsymbol{0}_{1\times 11}\\ -\boldsymbol{M}^{-1}\boldsymbol{E}_{\boldsymbol{u}}\end{bmatrix},\quad \boldsymbol{B}_{\boldsymbol{d}}=\begin{bmatrix}\boldsymbol{0}_{1\times 11}\\ -\boldsymbol{E}\end{bmatrix},\quad \boldsymbol{C}=\boldsymbol{I}_{22},\\ \boldsymbol{E}=\begin{bmatrix}1\\ 1\\ \vdots\\ 1\end{bmatrix},\quad \boldsymbol{E}_{\boldsymbol{u}}=\begin{bmatrix}1\\ 0\\ \vdots\\ 0\end{bmatrix}.\end{cases} \tag{6}$$

In the above equations, $\boldsymbol{I_n}$ is the $n \times n$ identity matrix, $\boldsymbol{B}$ is the input matrix for active control, which indicates the placement of active-control devices, $\boldsymbol{B_d}$ is the input matrix for an earthquake, and $\boldsymbol{C}$ is the output matrix that shows the locations of the sensors. If all states are measured, then $\boldsymbol{C}$ is an identity matrix.

This study used the following feedback control law

$$\boldsymbol{u}(t) = \boldsymbol{K_P}\boldsymbol{z}(t), \tag{7}$$

where $\boldsymbol{K_P}$ is the state-feedback gain that is designed by minimizing the following performance index

$$J = \int_0^\infty \left\{ \boldsymbol{z}^{\mathrm{T}}(t)\,\boldsymbol{Q}\boldsymbol{z}(t) + \boldsymbol{u}^{\mathrm{T}}(t)\boldsymbol{R}\boldsymbol{u}(t) \right\} dt \tag{8}$$

The block diagram of the control system containing (5) and (7) is shown in Fig. 3.

A performance index that considers the absolute acceleration, the inter-story drift, and the inter-story drift velocity, which is AD-LQR, is defined as follows [31]:

$$J = \int_0^\infty \left\{ \begin{bmatrix} \boldsymbol{\Delta x}(t) & \boldsymbol{\Delta \dot{x}}(t) \end{bmatrix}^{\mathrm{T}} \boldsymbol{Q_d} \begin{bmatrix} \boldsymbol{\Delta x}(t) \\ \boldsymbol{\Delta \dot{x}}(t) \end{bmatrix} + \left[\ddot{\boldsymbol{x}}(t) + \ddot{\boldsymbol{x}}_{\boldsymbol{g}}(t) \right]^{\mathrm{T}} \boldsymbol{Q_g} \left[\ddot{\boldsymbol{x}}(t) + \ddot{\boldsymbol{x}}_{\boldsymbol{g}}(t) \right] + \boldsymbol{u}^{\mathrm{T}}(t)\boldsymbol{R_u}\boldsymbol{u}(t) \right\} dt, \tag{9}$$

where $\boldsymbol{Q_d} = \mathrm{diag}\{q_{d1} \quad q_{d2} \quad \dots \quad q_{d22}\}$ is the weighting matrix for the inter-story drifts and velocity of each story, $\boldsymbol{Q_g} = \mathrm{diag}\{q_{g1} \quad q_{g2} \quad \dots \quad q_{g11}\}$ is the weighting matrix for the absolute acceleration of each story, and $\boldsymbol{\Delta x}(t) = [\Delta x_1(t) \quad \Delta x_2(t) \quad \dots \quad \Delta x_{11}(t)]$ is the vector of the inter-story drift of each story. In this equation, the i-th story inter-story drift is given by the following equation:

$$\begin{cases} \Delta x_i = x_1, & i = 1 \\ \Delta x_i = x_i - x_{i-1} & i = 2,3,...,n. \end{cases} \tag{10}$$

There exists a nonsingular matrix, $\boldsymbol{\Gamma}$, such that

$$\begin{bmatrix} \boldsymbol{\Delta x}(t) \\ \boldsymbol{\Delta \dot{x}}(t) \end{bmatrix} = \boldsymbol{\Gamma} \begin{bmatrix} \boldsymbol{x}(t) \\ \dot{\boldsymbol{x}}(t) \end{bmatrix}, \quad \boldsymbol{\Gamma} = \begin{bmatrix} 1 & & & \\ -1 & 1 & & \\ \vdots & & \ddots & \\ 0 & \dots & -1 & 1 \end{bmatrix}. \tag{11}$$

Rewriting (5) gives

$$\ddot{\boldsymbol{x}}(t) + \ddot{\boldsymbol{x}}_{\boldsymbol{g}}(t)\boldsymbol{E} = \boldsymbol{\Xi}\,\boldsymbol{z}(t) + \boldsymbol{\Psi}\boldsymbol{u}(t), \tag{12}$$

where $\boldsymbol{\Xi} = \left[-\boldsymbol{M}^{-1}\boldsymbol{K} \quad -\boldsymbol{M}^{-1}\boldsymbol{D} \right]$ and $\boldsymbol{\Psi} = -\boldsymbol{M}^{-1}\boldsymbol{E_u}$,

Substituting (11) into (9) yields

$$J = \int_0^\infty \left\{ \boldsymbol{z}^{\mathrm{T}}(t)\boldsymbol{Q}\boldsymbol{z}(t) + 2\boldsymbol{z}(t)\boldsymbol{S}\boldsymbol{u}(t) + \boldsymbol{u}^{\mathrm{T}}(t)\boldsymbol{R}\boldsymbol{u}(t) \right\} dt, \tag{13}$$

where

$$\boldsymbol{Q} = \boldsymbol{\Gamma} \boldsymbol{Q}_d \boldsymbol{\Gamma} + \boldsymbol{\Xi}^{\mathrm{T}} \boldsymbol{Q}_g \boldsymbol{\Xi}\,, \tag{14}$$

$$2\boldsymbol{z}(t)\boldsymbol{S}\boldsymbol{u}(t) = -\boldsymbol{z}^{\mathrm{T}}(t)\boldsymbol{\Xi}^{\mathrm{T}}\boldsymbol{Q}_g\boldsymbol{\Psi}\boldsymbol{u}(t) + \boldsymbol{u}^{\mathrm{T}}(t)\boldsymbol{\Psi}^{\mathrm{T}}\boldsymbol{Q}_g\boldsymbol{\Xi}\boldsymbol{z}(t)\,, \tag{15}$$

$$\boldsymbol{R} = \boldsymbol{\Psi}^{\mathrm{T}}\boldsymbol{Q}_g\boldsymbol{\Psi} + \boldsymbol{R}_u \,. \tag{16}$$

Minimizing (13) yields the state-feedback gain

$$\boldsymbol{K}_P = -\boldsymbol{R}^{-1}\left(\boldsymbol{S}^{\mathrm{T}} + \boldsymbol{B}_u^{\mathrm{T}}\boldsymbol{P}\right), \tag{17}$$

where P is the positive symmetrical solution of the following Riccati equation

$$\left\{\boldsymbol{A} - \boldsymbol{B}_u\boldsymbol{R}^{-1}\boldsymbol{S}^{\mathrm{T}}\right\}^{\mathrm{T}}\boldsymbol{P} + \boldsymbol{P}\left\{\boldsymbol{A} - \boldsymbol{B}_u\boldsymbol{R}^{-1}\boldsymbol{S}^{\mathrm{T}}\right\} + \boldsymbol{Q} - \boldsymbol{P}\boldsymbol{B}_u\boldsymbol{R}^{-1}\boldsymbol{B}_u^{\mathrm{T}}\boldsymbol{P} - \boldsymbol{S}\boldsymbol{R}^{-1}\boldsymbol{S}^{\mathrm{T}} = \boldsymbol{0}_{2n\times 2n}\,. \tag{18}$$

3. Selecting weighting matrices using BO method

This section shows how the BO method is used for the selection of weighting matrices in (11). Moreover, the Gaussian process used in BO is also explained.

3.1 Formulation of weight selection problem

The state-feedback gain, $\boldsymbol{K}_p$, which is designed by optimizing the performance index (9), is described as

$$\boldsymbol{K}_p = LQR(\boldsymbol{A}, \boldsymbol{B}, \boldsymbol{Q}_d, \boldsymbol{Q}_g, \boldsymbol{R}) \,. \tag{19}$$

Introducing a parameter vector, θ, allows us to parameterize the weighting matrices of $\boldsymbol{Q}_d$ and $\boldsymbol{Q}_g$. This study formulated the optimization problem as

$$\boldsymbol{K}_p(\boldsymbol{\theta}) = LQR(\boldsymbol{A}, \boldsymbol{B}, \boldsymbol{W}_d(\boldsymbol{\theta}), \boldsymbol{W}_g(\boldsymbol{\theta}), \boldsymbol{R})\,, \tag{20}$$

where $\boldsymbol{W}_d(\boldsymbol{\theta})$ and $\boldsymbol{W}_g(\boldsymbol{\theta})$ are positive symmetric matrices.

For this optimization problem, an earthquake is selected to design the state-feedback gain. This study searched the weight, $\boldsymbol{\theta}$, by minimizing the absolute acceleration under the selected earthquake. The constraint of the optimization is the maximum displacement of the PBI in the allowable range. The optimization problem is described as follows:

$$\begin{aligned} &\arg\min_{\theta\in R^n} \ \boldsymbol{A}_C(\boldsymbol{\theta}) = (\boldsymbol{A}, \boldsymbol{B}, \boldsymbol{K}_p(\boldsymbol{\theta})) \\ &s.t. \ \ \max \boldsymbol{D}_0(\boldsymbol{\theta}) <_a \boldsymbol{D}_0, \end{aligned} \tag{21}$$

where $\boldsymbol{A}_C(\boldsymbol{\theta})$ and $\max \boldsymbol{D}_0(\boldsymbol{\theta})$ are the maximum absolute acceleration and the maximum inter-story displacement of the PBI for preselected earthquakes, respectively; and ${}_a\boldsymbol{D}_0$ is the allowable maximum displacement of the PBI story.

3.2. Gaussian process and model estimation

Processes $\left((\boldsymbol{f}(\boldsymbol{\theta}_1),\boldsymbol{\theta}_1),\ (\boldsymbol{f}(\boldsymbol{\theta}_2),\boldsymbol{\theta}_2),...,(\boldsymbol{f}(\boldsymbol{\theta}_n),\boldsymbol{\theta}_n),\right)$ are Gaussian processes (GPs) if the combination of every process follows the Gaussian distribution. A GP is specified by a mean function, $\boldsymbol{\mu}_f$, and a covariance matrix, $\boldsymbol{K}_c$. If $\boldsymbol{f}(\boldsymbol{\theta})$ follows the GP, then the process is expressed as follows:

$$\boldsymbol{f}(\boldsymbol{\theta}) \sim GP(\boldsymbol{\mu}_f(\boldsymbol{\theta}),\ \boldsymbol{K}_C(\boldsymbol{\theta},\boldsymbol{\theta}')). \tag{22}$$

In (20), $\boldsymbol{\mu}_f(\boldsymbol{\theta})$ can be chosen to be 0, $\boldsymbol{\theta}'$ is an arbitrary input, and $\boldsymbol{K}_C$ is given by

$$\boldsymbol{K}_C(\boldsymbol{\theta},\boldsymbol{\theta}') = \boldsymbol{\sigma}_f^2 \exp\left(-\frac{1}{2}(\boldsymbol{\theta}-\boldsymbol{\theta}')^{\mathrm{T}}\boldsymbol{\Sigma}^{-1}(\boldsymbol{\theta}-\boldsymbol{\theta}')\right), \tag{23}$$

where $\boldsymbol{\sigma}_f^2$ is the prior variance of $f(\boldsymbol{\theta})$ and $\boldsymbol{\Sigma}$ is a variance-covariance matrix.

Subsection 3.1 formulated the optimization problem for the selection of the LQR weighting matrices. Since this problem needs to solve a multidimensional differential equation, and the state-feedback gain is given by solving a high dimensioned Riccati equation, which is nonlinear, the relationship between $\boldsymbol{\theta}$ and $\boldsymbol{A}_c(\boldsymbol{\theta})$ is complex. Thus, it is difficult to use an analytical optimization method to find a solution. This study estimated the model of the relationship between $\boldsymbol{\theta}$ and $\boldsymbol{A}_c(\boldsymbol{\theta})$ using the Gaussian process, and used it for optimization.

The estimated value of $\boldsymbol{A}_c(\boldsymbol{\theta})$, $\widetilde{\boldsymbol{A}}_C(\boldsymbol{\theta})$ is described by

$$\widetilde{\boldsymbol{A}}_C(\boldsymbol{\theta}) = \boldsymbol{A}_C(\boldsymbol{\theta}) + \boldsymbol{\varepsilon} \tag{24}$$

where $\boldsymbol{\varepsilon} \sim N(0,\ \sigma_\varepsilon^2)$ is a Gaussian noise, and $N(0,\ \sigma_\varepsilon^2)$ is a Gaussian distribution with the average being zero and the variance being σ_ε^2.

An arbitrary input vector $\boldsymbol{\theta}_* = [\boldsymbol{\theta}_{*1},...,\boldsymbol{\theta}_{*n}]$ is used for training, and the output of the vector, $\boldsymbol{A}_C(\boldsymbol{\theta}_*) = [\boldsymbol{A}_C(\boldsymbol{\theta}_{*1}),...,\boldsymbol{A}_C(\boldsymbol{\theta}_{*n})]$, is set to calculate the prior average and variance of the objective function, $A_c(\theta_*)$. The estimated Gaussian distribution is

$$p(\boldsymbol{A}_C(\boldsymbol{\theta}_*) \mid \Phi,\boldsymbol{\theta}) \sim N(\mu(\boldsymbol{\theta}_*),\ \boldsymbol{\sigma}^2(\boldsymbol{\theta}_*)), \tag{25}$$

where $\Phi = \{\boldsymbol{\theta}_*,\ \boldsymbol{A}_C(\boldsymbol{\theta}_*)\}$ is a data set.

The mean function, $\mu(\theta_*)$, and variance, $\boldsymbol{\sigma}^2(\boldsymbol{\theta}_*)$, are given by

$$\boldsymbol{\sigma}(\boldsymbol{\theta}_*) = \boldsymbol{K}_C(\boldsymbol{\theta}_*,\boldsymbol{\theta}_*) - \boldsymbol{K}_C(\boldsymbol{\theta}_*,\boldsymbol{\theta})\left\{\boldsymbol{K}_C(\boldsymbol{\theta},\boldsymbol{\theta}) + \boldsymbol{\sigma}_f^2\boldsymbol{I}\right\}\boldsymbol{K}_C(\boldsymbol{\theta},\boldsymbol{\theta}_*), \tag{26}$$

$$\mu(\boldsymbol{\theta}_*) = \boldsymbol{K}_C(\boldsymbol{\theta}_*,\boldsymbol{\theta})\left\{\boldsymbol{K}_C(\boldsymbol{\theta},\boldsymbol{\theta}) + \boldsymbol{\sigma}_f^2 I\right\}\widetilde{\boldsymbol{A}}_C(\boldsymbol{\theta}_*). \tag{27}$$

3.3. Bayesian optimization

BO searches a global optimal value without requiring the calculation of the gradient of an objective function. Since this method is a nonparametric optimization method, a prior objective function is not required to calculate an optimal value.

This optimization method iteratively updates the parameter, $\boldsymbol{\theta}_{new}$, and the objective function, $\boldsymbol{A}_C(\boldsymbol{\theta}_{new})$. This data is used to renew the estimation, $\widetilde{\boldsymbol{A}}_C(\boldsymbol{\theta}_{new})$.

The model estimated by the Gaussian process needs a prior distribution, average, and variance. Initial parameters, $\boldsymbol{\theta}_*$, are randomly chosen to yield sample values for calculation.

The updated point, $\boldsymbol{\theta}_{new}$, is obtained by maximizing an acquisition function, $\alpha(\boldsymbol{\theta}_{new})$:

$$\boldsymbol{\theta}_{new} = \text{argmax}\ \alpha(\boldsymbol{\theta}_{*}) \tag{28}$$

Many types of acquisition functions have been presented, such as the Kullback-Leibler divergence [18] and the probability of improvement [25, 26].

This study used the following probability of improvement of the objective function as the acquisition function:

$$\alpha(\boldsymbol{\theta}) = E_{\rho}[\max(0,\ \mu_{\rho}(\boldsymbol{\theta}_{best}) - \widetilde{\boldsymbol{A}}_{\boldsymbol{C}}(\boldsymbol{\theta})]\ , \tag{29}$$

where $\mu_{\rho}(\boldsymbol{\theta})$ is the mean function of the posterior distribution, $\boldsymbol{\theta}_{best}$ is the location that optimizes the objective function, and $\mu_{\rho}(\boldsymbol{\theta}_{best})$ is the average of $\boldsymbol{\theta}_{best}$.

The algorithm of the BO method is shown in Fig. 4.

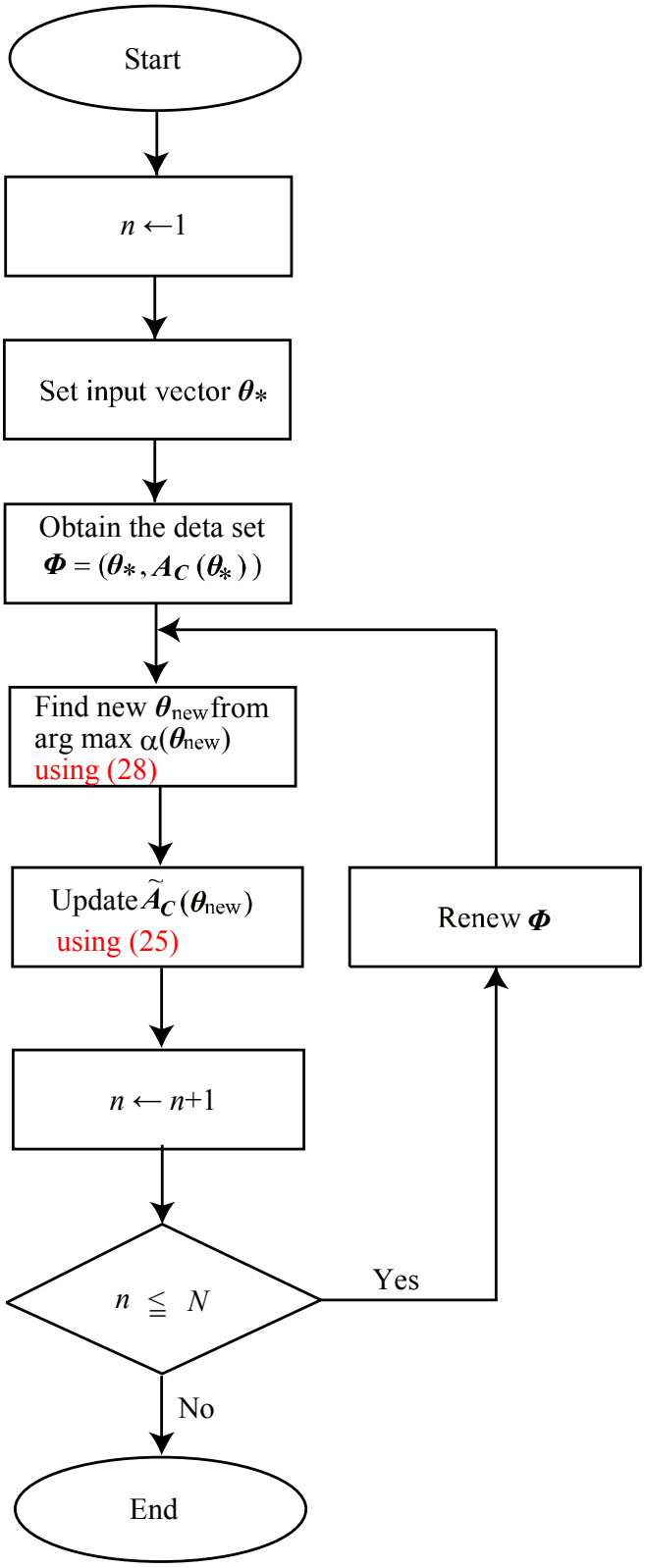

Fig. 4. Algorithm of the BO method

4. Numerical verification

This section uses the model given in Section 2 and three earthquake accelerograms to demonstrate the validity of the BO method for the weight selection in the design of the state-feedback gain.

4.1. Earthquake waves

An artificial earthquake accelerogram (Art Hachinohe wave) and two recorded earthquake accelerograms (Kobe and El-Centro waves) are used to assess the performance of the vibration control method:

1. Art Hachinohe wave: the spectrum of the pseudo velocity response, ${}_pS_v$, is 100 cm/s after a corner period of 0.64 s for a building with damping ratio of 5%, and the phase characteristic is the same as the earthquake wave of 1968 Hachinohe EW.
2. Kobe wave：JMA Kobe NS 1995.
3. El-Centro wave：El-Centro NS 1940.

The accelerograms and the spectrums of the pseudo velocity responses of these three waves are shown in Figs. 5–8. Art Hachinohe wave is used to design the state-feedback gain, and Kobe and El-Centro waves are used to verify the design results.

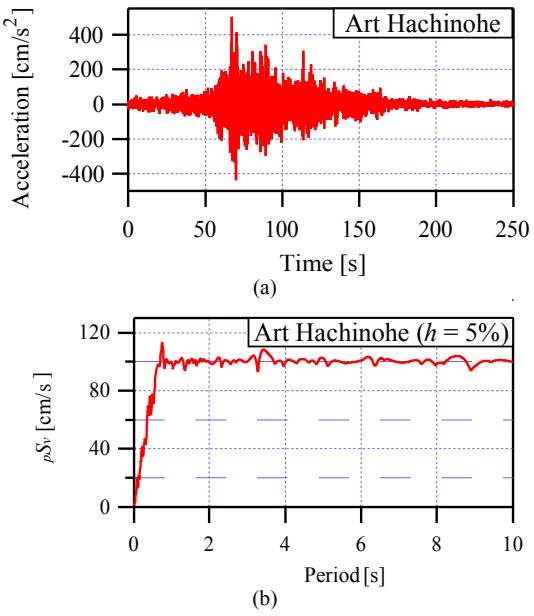

Fig. 5. Art Hachinohe wave (a): accelerogram and (b): pseudo velocity spectrum.

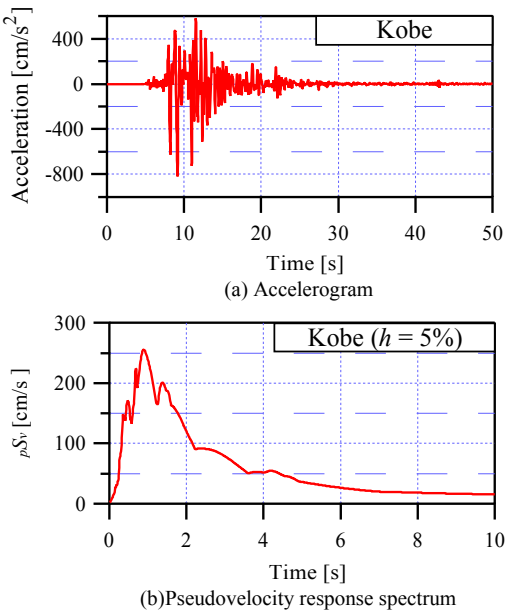

Fig. 6. Kobe wave (a): accelerogram and (b) : pseudo velocity spectrum

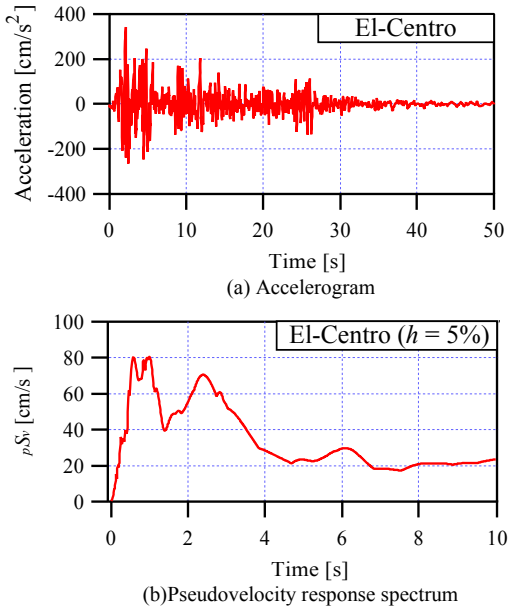

Fig. 7. El-Centro wave (a): accelerogram and (b): pseudo velocity spectrum.

4.2. Optimization of two parameters (LQR-2V)

As the first step, the optimization of two parameters for the LQR control is used to illustrate the validity of the BO method, and the exhaustive search method is employed for comparison. This LQR system is called LQR-2V for the remainder of the manuscript. The weighting matrices, $\boldsymbol{Q}_d$ and $\boldsymbol{Q}_g$, are used for the inter story drift and velocity, and the absolute acceleration, respectively. Two parameters, α and β, are introduced to simplify the selection of the weighting matrices, which are chosen from the range [0, 15]:

$$\boldsymbol{Q}_d = 10^{\alpha}\boldsymbol{I}_{22}, \text{ and } \boldsymbol{Q}_g = 10^{\beta}\boldsymbol{I}_{11}, \tag{30}$$

The objective function for the LQR design is chosen to be the maximum absolute acceleration of the building for Art Hachinohe wave. The constraint is

$$|x_0(t)| \le 55\,\text{cm}, \tag{31}$$

that is, the displacement of the PBI story must be less than 55 cm. This is a commonly used clearance for buildings in Japan [32].

For the exhaustive search method, a step size is set to be 0.1 for both α and β in [0, 15] to perform the search. It yields 22,500 sets of state-feedback gains. The relationship between the maximum absolute acceleration and the parameters of α and β for Art Hachinohe wave (Fig. 8) show that the optimal values of the parameters are

$$\alpha = 14.2 \text{ and } \beta = 14.7. \tag{32}$$

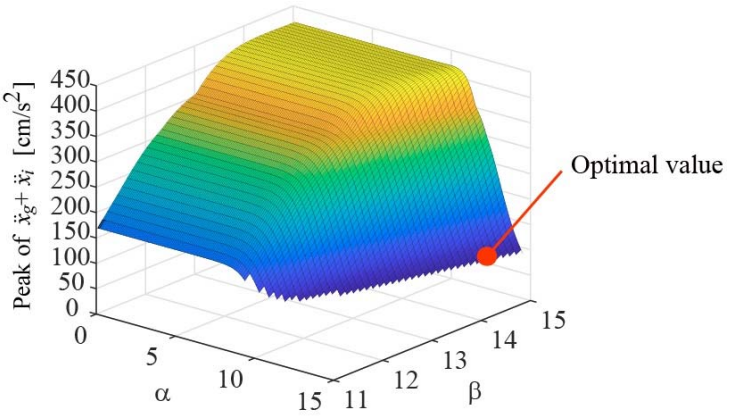

Fig. 8. Relationship between maximum absolute acceleration and parameters, α and β, for a state-feedback gain given by exhaustive search method.

A prior distribution and average of the absolute acceleration are needed for BO. This study initially chose 10 random samples to calculate those values. The search was performed on a personal computer (CPU: Inter (R) Core (TM) i7-4790 Processor 3.6 GHz, RAM: 16 GB). The total search time was 700 s. The relationship between the objective function (the absolute acceleration) and the iteration number (Fig. 9) shows that the objective function decreases fast at the beginning of iteration, and enters into the steady state at the 55th iteration. Thus, a 200 iteration search is sufficient to find an optimal value for LQR-2V. The result of the BO is shown in Fig. 10. In the figure, the blue dots indicate search points, and the green area does not satisfy Constraint (31).

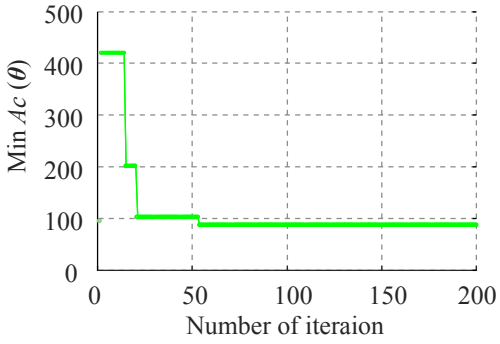

Fig.9. Result of the searching of LQR-2V

BO gives the optimal parameters

$$\alpha = 14.3, \beta = 14. \tag{33}$$

These values are very close to those of the exhaustive search method.

It is clear from Fig 10 that the BO method intensively and efficiently searched a solution around the optimal area.

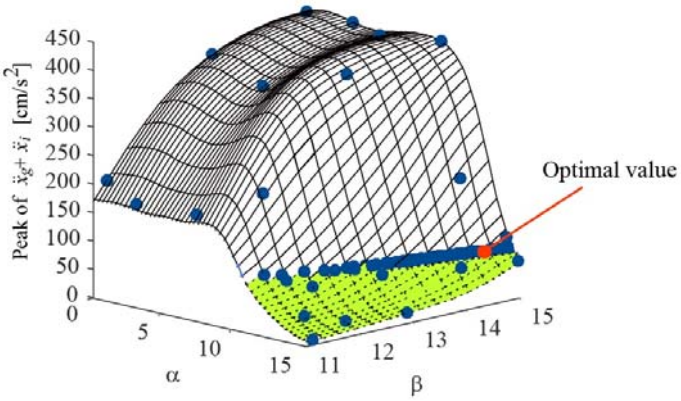

Fig.10. Relationship between maximum absolute acceleration and parameters, α and β, for a state-feedback gain given by BO method.

The inter-story drift angle and the story-shear coefficient of the i-th story are given by

$$\begin{cases} \theta_i = \arctan\dfrac{\Delta x_i}{h_i} \approx \dfrac{\Delta x_i}{h_i}, \\ c_i = \dfrac{\left|\sum_{j=i}^{10} f_j\right|}{\sum_{j=i}^{10} m_j g}, \end{cases} \tag{34}$$

where f_i is the story shear of the i-th story.

The average of the maximum displacement, absolute acceleration, inter-story drift angle, and the story-shear coefficient response of each story for the 10 sets are shown in Fig. 11. In the figure, 0 is

the PBI story, and g is the ground. Table 1 shows the average standard deviation of each story for each response.

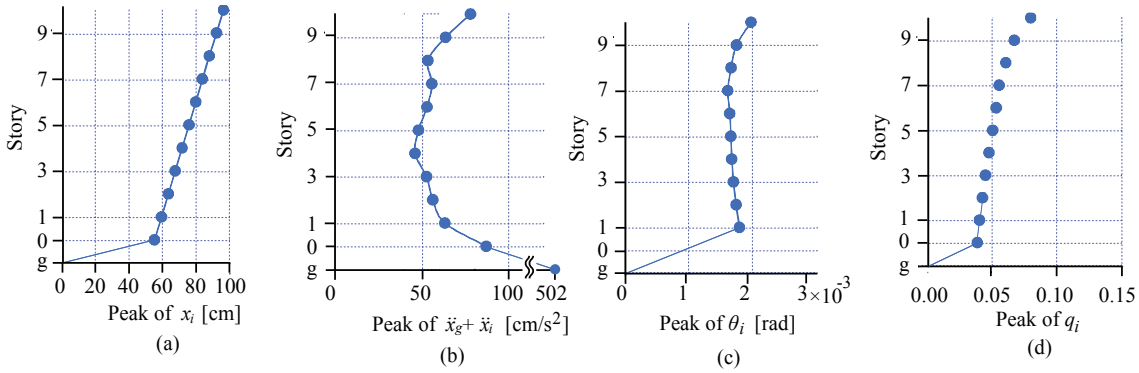

Fig.11. Average of maximum (a) displacement, (b) absolute acceleration, (c) inter-story drift angle, and (d) story-shear coefficient of LQR-2V for 10 sets.

Table 1. Average standard deviation for each response

Displacement [cm]	Absolute acceleration [cm/s^2]	Inter-story-drift angle [rad]	Story-shear coefficient
0.012	0.011	1.55×10^{-7}	5.07×10^{-6}

It is clear from Fig. 11 and Table 1 that the average standard deviation values for the 10 sets are very small.

The comparison between Figs. 8 and 10, (32) and (33), and the above explanations, reveal that the BO method can be used to find optimal weighting matrices for the design of an optimal feedback control gain.

4.3. Optimization of thirty-three parameters (LQR-33V)

Utilizing the confidence gained by applying the BO method for the optimal selection of weighting matrices given in the previous subsection, we perform a finite search for the weighting matrices using the BO method in this subsection.

The weighting matrices, $\boldsymbol{Q_d}$ and $\boldsymbol{Q_g}$, are set to be

$$\boldsymbol{Q_d} = 10^{\mathrm{diag}\{q_{d1} \;\; q_{d2} \;\; \cdots \;\; q_{d22}\}} \text{ and } \boldsymbol{Q_g} = 10^{\mathrm{diag}\{q_{g1} \;\; q_{g2} \;\; \cdots \;\; q_{g11}\}}. \tag{35}$$

The weighting matrices are set to be the inter-story drift, velocity, and absolute acceleration of each story. This LQR system is called LQR-33V in this study. This subsection considers the same objective function and constraint as that in the previous subsection.

The search was performed by setting N = 500. The optimization was run 50 times and the resulting 50 sets of optimal gains were used for the analysis of the method.

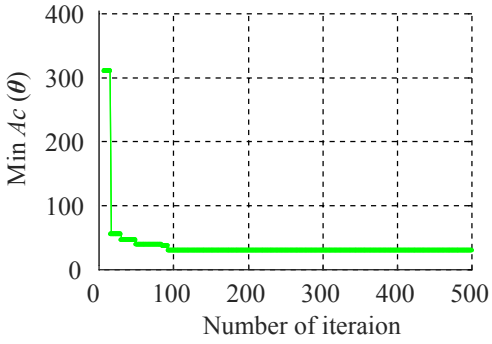

Fig. 12. Result of the searching of LQR-33V

The situation of the convergence of the BO method (Fig. 12) shows that the object function decreases quickly in the beginning, then the decreasing speed gradually decreases, and finally it reaches the minimum and remains unchanged from the 93th iteration onward. This shows that 500 iterations are sufficient to find an optimal value for the optimization problem. It took 35,000 s for the search to complete.

The average of the displacement, absolute acceleration, inter-story drift angle, and the story-shear coefficient of each story for the 50 sets are shown in Fig. 13 with error bars, and the variations are clearly small. Since the constraint is set for the PBI story, the variations of the absolute acceleration, displacements, and the story-shear coefficients at lower stories are smaller than those for the upper stories.

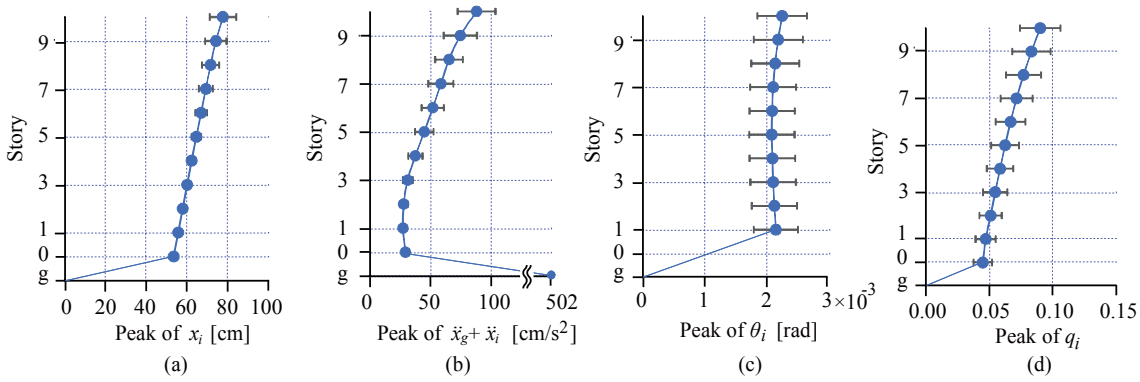

Fig. 13. Average of maximum (a) displacement, (b) absolute acceleration, (c) inter-story drift angle, and (d) story-shear coefficient of LQR-33V for 50 sets.

However, the variations of the inter-story drift angles are almost the same for each story. The reason for this can be explained by the fact that the structural model employed a base isolation. This caused the influence of the first mode to be much larger than the others. Moreover, the stiffness of the superstructure was designed using the straight-line mode (1). This results in that the variations of

the absolute acceleration, displacements, and the story-shear coefficients is much smaller for lower stories than for the upper stories.

4.4. Comparison between LQR-2V, LQR-33V, and the conventional method

A comparison between the optimization of 2 parameters (LQR-2V), 33 parameters (LQR-33V), and conventional methods (LQRs 1 [7] and 2 [17]), and no control (NC) is carried out. The weighting matrices of LQRs 1 and 2 are set to be

$$\text{LQR1}: \boldsymbol{Q} = 10^{\chi}\begin{bmatrix} \boldsymbol{K} & \boldsymbol{0}_{n\times n} \\ \boldsymbol{0}_{n\times n} & \boldsymbol{M} \end{bmatrix}, \quad \boldsymbol{R} = 1, \tag{36}$$

$$\text{LQR2}: \boldsymbol{Q} = \boldsymbol{I}_{11}, \quad \boldsymbol{R} = 10^{-\delta}. \tag{37}$$

Note that the maximum displacements of the base isolation story for LQR-2V and LQR-33V are almost the same. The weighting matrices of LQRs 1 and 2 (Table 2) are also selected such that the maximum displacements of the base isolation story have the same level.

Table. 2. Selected weighting matrices

LQR-2V	$\boldsymbol{Q}_g = 10^{\alpha}\boldsymbol{I}_{11}$ and $\boldsymbol{Q}_g = 10^{\beta}\boldsymbol{I}_{11}$,	α = 14.3 and β = 14.
LQR-33V	$\boldsymbol{Q}_d = 10^{\text{diag}\{q_{d1} \;\; q_{d2} \;\; \cdots \;\; q_{d22}\}}$ and $\boldsymbol{Q}_g = 10^{\text{diag}\{q_{g1} \;\; q_{g2} \;\; \cdots \;\; q_{g11}\}}$	q_{d1} = 4.22, q_{d2} = 11.18, q_{d3} = 10.91, q_{d4} = 4.34, q_{d5} = 7.65, q_{d6} = 8.56, q_{d7} = 10.30, q_{d8} = 10.92, q_{d9} = 6.20, q_{d10} = 8.71, q_{d11} = 5.37, q_{d12} = 14.44, q_{d13} = 11.23, q_{d14} = 3.45, q_{d15} = 14.98, q_{d16} = 4.18, q_{d17} = 2.52, q_{d18} = 6.38 q_{d19} = 8.26, q_{d20} = 12.78, q_{d21} = 0.72, q_{d22} = 5.53, q_{g1} = 14.98, q_{g2} = 7.85, q_{g3} = 0.66, q_{g4} = 0.50, q_{g5} = 0.95, q_{g6} = 8.02, q_{g7} = 4.63, q_{g8} = 4.99, q_{g9} = 10.71, q_{g10} = 4.23, and q_{g11} = 0.40.
LQR1	$\boldsymbol{Q} = 10^{\chi}\begin{bmatrix} \boldsymbol{K} & \boldsymbol{0}_{n\times n} \\ \boldsymbol{0}_{n\times n} & \boldsymbol{M} \end{bmatrix}$ and $\boldsymbol{R} = 1$	χ = 4.9
LQR2	$\boldsymbol{Q} = \boldsymbol{I}_{11}$ and $\boldsymbol{R} = 10^{-\delta}$	δ = –9.4

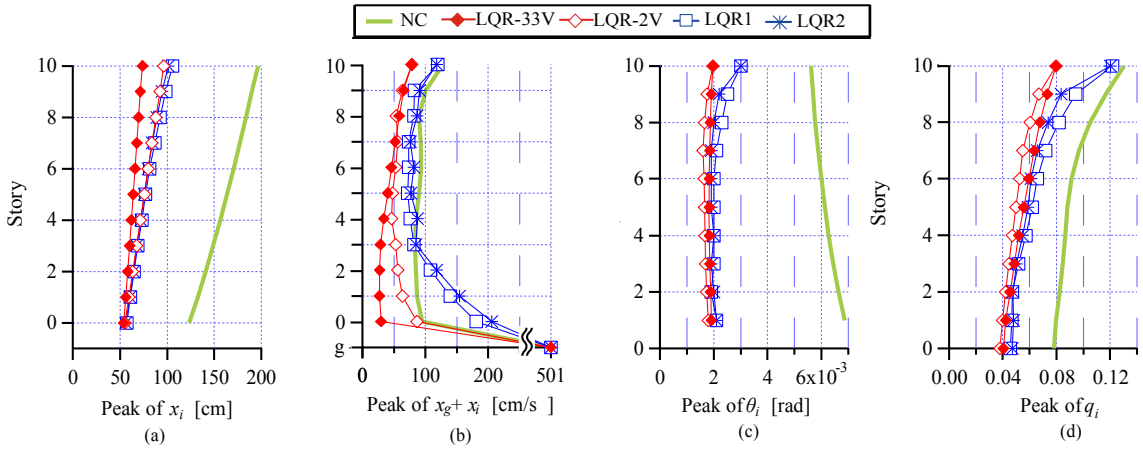

Fig. 14. Results for Art Hachinohe wave

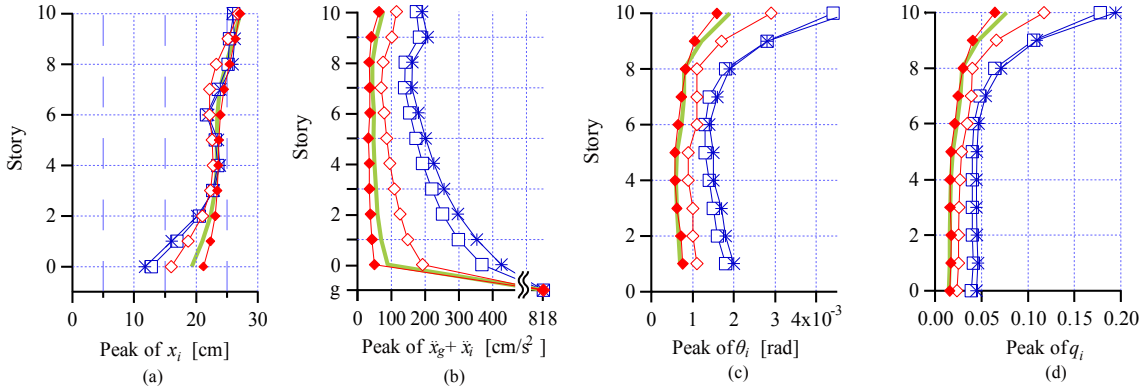

Fig. 15. Results for Kobe wave

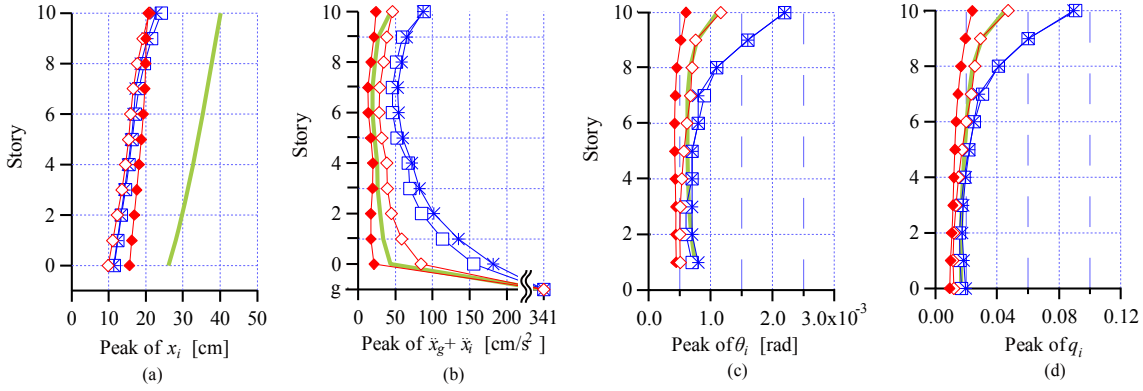

Fig. 16. Results for El-Centro wave

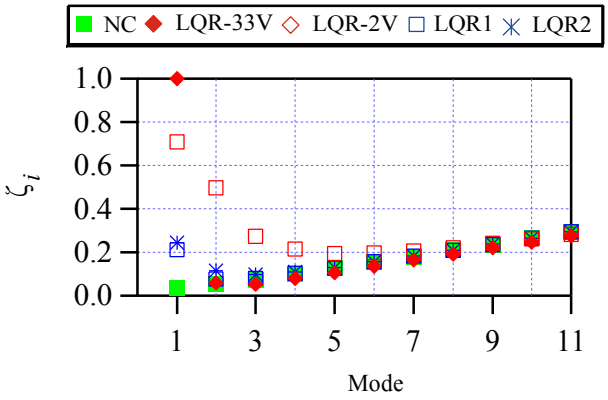

Fig. 17. Damping ratio for each mode of NC, LQR-33V, LQR-2V, LQR1, LQR2, and NC

The responses obtained for Art Hachinohe wave, Kobe wave, and El-Centro wave are shown in Figs. 14–16, and the detailed data from Figs. 14–16 are shown in Appendix.

The maximum displacement of each story for LQR-2V, LQR-33V, LQR 1, and LQR 2 [(a) in Figs. 14-16] were all in the allowable range; that is, Constraint (29) was satisfied.

The maximum absolute acceleration of LQR-2V, LQR-33V, LQR 1, and LQR 2, and NC for the three earthquake waves are shown in (b) in Figs. 14–16. Since the performance index of LQR-2V included the absolute acceleration, the absolute acceleration for LQR-2V was better than that for LQRs 1 and 2, especially for the lower stories. The absolute acceleration of the LQR-2V for Kobe wave was bigger than that of the NC. The reason might be that the weighting matrices of LQR-2V only have two parameters. Thus, the number of parameters was not enough to produce a satisfactory controller. In contrast, the absolute acceleration of the LQR-33V was smaller than that of the LQR-2V and NC.

For Art Hachinohe wave, the maximum absolute acceleration of the PBI story is 80 cm/s^2 for LQR-2V, and 40 cm/s^2 for LQR-33V. Thus, LQR-33V suppressed it to approximately 50% of that for the LQR-2V. LQR-33V suppressed it to approximately 75% of that for the LQR-2V for Kobe wave, and approximately 70% for El-Centro wave. The simulation results show that even if the performance index included the absolute acceleration, if the performance index does not have enough parameters for tuning, the controller may not achieve the desired control performance.

The maximum inter-story drift angles of LQR-2V, LQR-33V, LQR 1, LQR 2, and NC are shown in (c) in Figs. 14–16 for the three earthquakes. The maximum inter-story-drift angles of LQR-2V and LQR-33V are almost the same, and are smaller than that of the LQR1 and LQR2 for Art Hachinohe wave [Fig. 14 (c)]. However, the 10th story inter-story-drift angle of LQR-33V is 50% smaller than that for the LQR-2V for the Kobe wave [Fig. 15 (c)] and El-Centro wave [Fig. 16 (c)].

As for the story shear coefficients of LQR-2V, LQR-33V, LQR1, LQR2, and NC for the three earthquakes, the maximum story shear coefficient of LQR-2V and LQR-33V are almost the same,

and are smaller than that of the LQR1 and LQR2 for Art Hachinohe wave [Fig. 14 (d)]. However, the LQR-33V suppresses the story shear coefficient at the 10th story to 50% of that for the LQR-2V for Kobe wave [Fig. 15 (d)] and El-Centro wave [Fig. 16 (d)].

The simulation results reveal that LQR-33V suppressed the absolute acceleration of the lower story more effectively than LQR-2V did. The maximum responses of the inter-story drift angles for the LQR-33V were smaller than that for the LQR-2V, especially at the upper stories.

The damping ratios of LQR-2V, LQR-33V, LQR 1 and LQR2 for each mode are shown in Fig. 17. Clearly, the damping ratios of the 2nd to 5th modes for LQR-2V are larger than that for LQR-33V, and the damping ratio of the 1st mode for LQR-33V is much bigger than that for the other controllers. Since a base isolation was employed under the building in this study, the influence of the 1st mode is bigger than that of the other modes. 33 parameters ensured a fine adjustment of a controller for a structural model.

The control inputs for these three earthquake waves are shown in Figs. 18–20, and Tables 3–5 show the maximum values of the power and the energy of the control inputs.

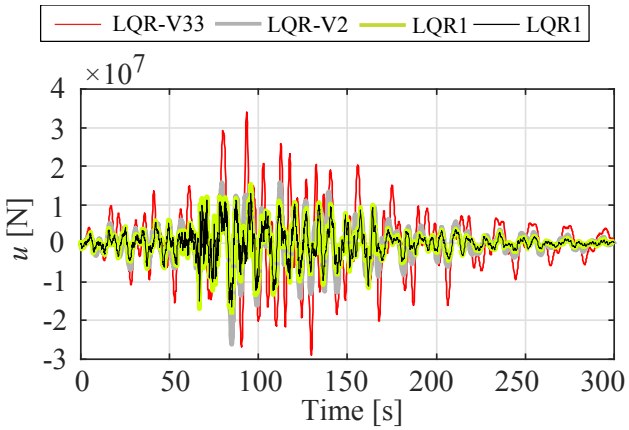

Fig.18. Control inputs for Art Hachinohe wave

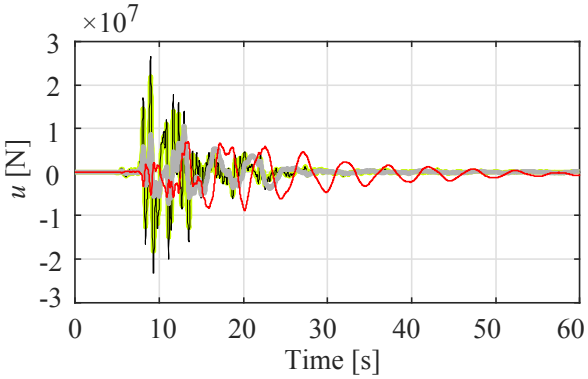

Fig. 19. Control inputs for Kobe wave

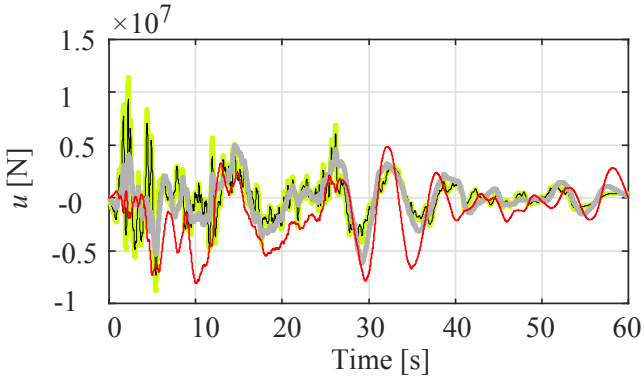

Fig. 20. Control inputs for El-Centro wave

Table 3. Max control

	Max control input [N](×10^7)		
	Art Hachinohe	Kobe	El-Centro
LQR-2V	2.62	1.06	0.61
LQR-33V	3.41	0.88	0.81
LQR1	1.9	2.66	1.14
LQR2	1.7	2.20	0.93

Table 4. Max energy

	Max energy [N·cm] (×10^8)		
	Art Hachinohe	Kobe	El-Centro
LQR-2V	101	6.40	3.74
LQR-33V	39.0	5.15	1.45
LQR1	105.4	12.55	4.77
LQR2	103.8	11.16	4.48

Table 5. Max power of control input.

	Max power [N·cm/s] (×10^8)		
	Art Hachinohe	Kobe	El-Centro
LQR-2V	11.0	5.97	1.37
LQR-33V	10.3	4.44	1.52
LQR1	9.3	11.82	2.36
LQR2	9.0	11.70	2.17

The control inputs for LQR-33V, LQR-2V, LQR 1, and LQR2 for the three earthquake waves are shown in Figs. 18–20. The maximum control input for Art Hachinohe wave was slightly bigger for LQR-33V than for LQR-2V (Fig. 18). And the maximum control inputs for Kobe and El-Centro waves were almost the same for LQR-33V and LQR-2V (Figs. 19 and 20).

The maximum power and energy of the control input of LQR-33V were smaller than that of the

LQR-2V, LQR1, and LQR2 (Tables 3 and 4). Basically, smaller control energy and power yielded a better control result for LQR-33V than for LQR-2V for the three earthquake waves (Figs. 14–17). Therefore, LQR-33V is more efficient than LQR-2V.

5. Conclusion

A linear quadratic regulator (LQR) is widely used in ASC. The suppression of both displacement and absolute acceleration is important to protect structures, people, and property. Since the design of an LQR contains a large number of parameters in the weighting matrices, it is important to find a way to simplify the selection of optimal parameters. This study considered the issue of selecting the weighting matrices of an LQR using the Bayesian optimization method (BO) for ASC for the first time. Unlike other methods, the weighting matrices were automatically selected by minimizing the response of the absolute acceleration generated by an earthquake. The maximum displacement of the passive-base-isolation (PBI) story was used as the constraint of the optimization. This method not only provides a powerful tool for LQR design, but also has the potential to be applied to other control problems, such as robust PID control.

A numerical example was used to examine the control performance for the relative displacement, absolute acceleration, inter-story-drift angles, story-shear, coefficients, damping ratio of each mode, and the energy and power of control input.

This study clarified the following points:

- The BO method automatically found LQR weighting matrices for active structural control, and the LQR control system that was designed by the weighting matrices suppressed not only the absolute, but also the acceleration and the inter story drift and velocity.
- An elaborate selection of all the thirty-three parameters of the weighting matrices (LQR-33V) yielded an optimal controller that provided us with satisfactory control performance. More specifically, while the maximum control input for LQR-33V was small enough, the control performance of the absolute acceleration, inter-story-drift angles, and the story-shear coefficients was satisfactory, and the control energy was also small.
- Unlike conventional methods, BO does not require any trial and error process to decide weights. Thus, even if a system is high-DOF, it is not difficult to design a controller.
- Since BO method finds optimal parameters by minimizing the objective function, the decided parameters are guaranteed to be optimal.

Appendix. Reponses for the Art Hachinohe, Kobe, and El-centro earthquakes

The detailed date of Figs. 14–16 are shown in Tables A.1-12.

A1. Maximum relative displacement for Art Hachinohe

	Maximum relative displacement of the stories [cm]										
	0	1	2	3	4	5	6	7	8	9	10
LQR-33V	54.1	56.1	58.0	60.0	61.9	63.8	65.8	67.7	69.6	71.5	73.8
LQR-2V	55.0	59.2	63.3	67.4	71.5	75.7	79.7	83.7	87.8	92.1	96.3
LQR1	56.1	60.3	64.1	67.8	71.8	75.8	79.5	83.9	89.0	94.4	100.9
LQR2	56.9	61.1	65.0	68.9	73.1	77.2	81.5	86.7	92.3	98.4	105.7
NC	123.5	132.4	140.8	148.8	156.4	163.7	170.6	177.1	183.5	189.9	196.7
LQR-33V /LQR-2V	98%	95%	92%	89%	87%	84%	83%	81%	79%	78%	77%
LQR-33V /NC	44%	42%	41%	40%	40%	39%	39%	38%	38%	38%	38%

A2. Maximum absolute acceleration for Art Hachinohe

	Maximum absolute acceleration of the stories [cm/s^2]										
	0	1	2	3	4	5	6	7	8	9	10
LQR-33V	29.4	26.9	27.0	28.4	33.9	40.1	45.9	51.9	58.3	65.7	77.9
LQR-2V	86.9	63.2	56.2	52.7	46.1	48.1	52.9	55.7	53.5	63.6	77.9
LQR1	205.6	154.9	117.8	84.7	87.5	76.3	82.0	76.1	86.3	90.9	117.9
LQR2	180.5	139.6	108.3	81.4	76.0	71.8	73.4	73.4	81.6	82.7	119.3
NC	95.2	86.9	84.9	83.6	85.5	90.3	92.9	92.5	89.6	101.0	127.6
LQR-33V /LQR-2V	34%	43%	48%	54%	73%	83%	87%	93%	109%	103%	100%
LQR-33V /NC	31%	31%	32%	34%	40%	44%	49%	56%	65%	65%	61%

A3. Maximum inter-story drift angle for Art Hachinohe

	Maximum inter-story-drift angle of the stories [rad]									
	0	2	3	4	5	6	7	8	9	10
LQR-33V	0.0019	0.0019	0.0019	0.0018	0.0018	0.0018	0.0018	0.0019	0.0019	0.0020
LQR-2V	0.0018	0.0017	0.0017	0.0017	0.0017	0.0016	0.0016	0.0017	0.0017	0.0020
LQR1	0.0021	0.0020	0.0019	0.0020	0.0019	0.0019	0.0019	0.0020	0.0022	0.0030
LQR2	0.0021	0.0019	0.0020	0.0020	0.0020	0.0020	0.0021	0.0023	0.0025	0.0030
NC	0.0036	0.0034	0.0032	0.0031	0.0029	0.0028	0.0028	0.0029	0.0030	0.0032
LQR-33V /LQR-2V	107%	108%	109%	110%	111%	112%	115%	113%	110%	100%
LQR-33V /NC	53%	55%	57%	60%	63%	65%	66%	64%	63%	61%

A4. Maximum story-shear coefficient for Art Hachinohe

	Maximum story-shear coefficient of the stories										
	0	1	2	3	4	5	6	7	8	9	10
LQR-33V	0.041	0.042	0.045	0.049	0.052	0.056	0.059	0.063	0.068	0.073	0.080
LQR-2V	0.038	0.040	0.042	0.044	0.047	0.050	0.053	0.055	0.060	0.067	0.080
LQR1	0.047	0.048	0.048	0.050	0.055	0.059	0.061	0.066	0.074	0.084	0.120
LQR2	0.046	0.047	0.047	0.052	0.057	0.062	0.066	0.072	0.082	0.094	0.122
NC	0.078	0.080	0.082	0.085	0.086	0.088	0.091	0.097	0.105	0.117	0.130
LQR-33V /LQR-2V	107%	106%	108%	109%	110%	111%	112%	115%	113%	110%	100%
LQR-33V /NC	52%	53%	55%	57%	60%	63%	65%	66%	64%	63%	61%

A5. Maximum relative displacement for Kobe

	Maximum relative displacement of the stories [cm]										
	0	1	2	3	4	5	6	7	8	9	10
LQR-33V	21.2	22.3	23.1	23.4	23.6	23.7	24.0	24.5	25.4	26.4	27.0
LQR-2V	16.0	18.7	21.0	22.3	22.8	22.6	22.2	22.2	23.3	25.1	26.8
LQR1	11.8	16.1	20.3	22.8	23.8	23.5	22.0	24.0	25.9	26.3	25.9
LQR2	12.7	16.9	20.6	22.7	23.5	23.1	21.7	23.6	25.2	25.4	26.1
NC	19.3	21.0	22.4	23.1	23.3	23.4	23.4	23.8	24.8	26.1	27.2
LQR-33V /LQR-2V	132%	119%	110%	105%	103%	105%	108%	110%	109%	105%	101%
LQR-33V /NC	110%	106%	103%	102%	101%	101%	102%	103%	102%	101%	100%

A6. Maximum absolute acceleration for Kobe

	Maximum absolute acceleration of the stories [cm/s^2]										
	0	1	2	3	4	5	6	7	8	9	10
LQR-33V	49.8	42.5	38.4	35.5	34.5	31.3	36.6	35.5	34.1	39.8	63.1
LQR-2V	191.6	148.0	124.8	108.5	96.0	86.2	79.0	69.7	75.7	100.9	115.2
LQR1	426.3	352.1	296.4	256.7	225.7	201.0	180.1	160.9	161.4	206.5	190.4
LQR2	368.3	299.0	251.9	218.6	192.8	172.2	154.7	138.6	141.3	182.5	174.3
NC	88.3	68.9	59.6	53.8	49.4	46.0	48.4	43.8	43.0	55.1	75.5
LQR-33V /LQR-2V	26%	29%	31%	33%	36%	36%	46%	51%	45%	39%	55%
LQR-33V /NC	56%	62%	65%	66%	70%	68%	75%	81%	79%	72%	84%

A7. Maximum inter-story drift angle for Kobe

	Maximum inter-story-drift angle of the stories [rad]									
	0	2	3	4	5	6	7	8	9	10
LQR-33V	0.0008	0.0007	0.0006	0.0006	0.0006	0.0007	0.0007	0.0008	0.0011	0.0016
LQR-2V	0.0011	0.0010	0.0010	0.0009	0.0009	0.0011	0.0011	0.0011	0.0017	0.0029
LQR1	0.0020	0.0018	0.0017	0.0015	0.0015	0.0014	0.0016	0.0019	0.0028	0.0048
LQR2	0.0018	0.0016	0.0015	0.0014	0.0013	0.0013	0.0014	0.0018	0.0028	0.0044
NC	0.0007	0.0007	0.0006	0.0006	0.0006	0.0007	0.0008	0.0008	0.0012	0.0019
LQR-33V /LQR-2V	69%	70%	64%	61%	61%	61%	64%	75%	62%	55%
LQR-33V /NC	109%	109%	99%	97%	91%	90%	92%	104%	86%	84%

A8. Maximum story-shear coefficient for Kobe

	Maximum story-shear coefficient of the stories										
	0	1	2	3	4	5	6	7	8	9	10
LQR-33V	0.016	0.017	0.017	0.016	0.016	0.017	0.021	0.025	0.030	0.041	0.064
LQR-2V	0.023	0.025	0.025	0.026	0.027	0.028	0.035	0.039	0.040	0.066	0.118
LQR1	0.045	0.046	0.045	0.045	0.044	0.045	0.047	0.054	0.071	0.110	0.194
LQR2	0.039	0.041	0.040	0.040	0.040	0.040	0.042	0.049	0.065	0.106	0.178
NC	0.015	0.016	0.016	0.017	0.017	0.019	0.024	0.027	0.029	0.047	0.077
LQR-33V /LQR-2V	68%	68%	69%	63%	61%	61%	61%	64%	75%	61%	55%
LQR-33V /NC	109%	107%	107%	98%	96%	91%	90%	92%	104%	86%	84%

A9. Maximum relative displacement for El-Centro

	Maximum relative displacement of the stories [cm]										
	0	1	2	3	4	5	6	7	8	9	10
LQR-33V	15.6	16.2	16.9	17.5	18.2	18.8	19.3	19.7	19.9	20.0	20.7
LQR-2V	9.8	11.1	12.3	13.5	14.6	15.3	15.8	16.5	17.6	19.2	20.9
LQR1	11.3	12.2	13.2	14.2	15.2	16.0	16.7	17.3	18.6	20.4	22.8
LQR2	11.5	12.4	13.4	14.4	15.4	16.3	17.1	18.0	19.6	21.6	24.1
NC	26.2	28.1	29.8	31.3	32.7	34.1	35.4	36.6	37.8	39.0	40.2
LQR-33V /LQR-2V	158%	147%	137%	129%	125%	123%	122%	119%	113%	104%	99%
LQR-33V /NC	59%	58%	57%	56%	55%	55%	55%	54%	53%	51%	51%

A10. Maximum absolute acceleration for El-Centro

	Maximum absolute acceleration of the stories [cm/s^2]										
	0	1	2	3	4	5	6	7	8	9	10
LQR-33V	21.2	17.2	16.9	19.4	19.5	16.9	13.6	13.3	17.1	21.1	23.8
LQR-2V	84.8	58.2	44.4	38.9	38.7	31.4	27.9	28.7	34.2	38.4	46.2
LQR1	181.7	135.1	102.1	82.4	72.2	60.1	54.0	52.7	58.2	65.7	87.6
LQR2	155.8	113.6	85.5	69.3	67.2	52.0	46.4	46.0	51.8	59.8	88.9
NC	43.6	33.8	29.3	26.2	25.9	21.9	19.3	19.2	22.6	27.3	44.4
LQR-33V /LQR-2V	25%	30%	38%	50%	50%	54%	49%	46%	50%	55%	52%
LQR-33V /NC	48%	51%	58%	74%	75%	77%	70%	69%	76%	77%	54%

A11. Maximum inter-story drift angle for El-Centro

	Maximum inter-story-drift angle of the stories [rad]									
	0	2	3	4	5	6	7	8	9	10
LQR-33V	0.00044	0.00044	0.00044	0.00043	0.00042	0.00042	0.00043	0.00045	0.00052	0.00060
LQR-2V	0.0005	0.0005	0.0005	0.0005	0.0006	0.0006	0.0007	0.0007	0.0008	0.0012
LQR1	0.0008	0.0007	0.0007	0.0007	0.0007	0.0008	0.0008	0.0011	0.0016	0.0022
LQR2	0.0007	0.0006	0.0006	0.0007	0.0007	0.0008	0.0009	0.0011	0.0016	0.0022
NC	0.0008	0.0007	0.0007	0.0006	0.0006	0.0006	0.0006	0.0007	0.0008	0.0011
LQR-33V /LQR-2V	87%	87%	85%	81%	75%	68%	64%	65%	68%	52%
LQR-33V /NC	59%	64%	67%	68%	68%	67%	68%	67%	65%	54%

A12. Maximum story-shear coefficient for El-Centro

	Maximum story-shear coefficient of the stories										
	0	1	2	3	4	5	6	7	8	9	10
LQR-33V	0.009	0.010	0.011	0.011	0.012	0.013	0.014	0.015	0.016	0.020	0.024
LQR-2V	0.012	0.011	0.012	0.014	0.015	0.017	0.020	0.023	0.026	0.029	0.047
LQR1	0.020	0.018	0.017	0.018	0.020	0.022	0.025	0.028	0.041	0.060	0.089
LQR2	0.017	0.016	0.016	0.017	0.019	0.022	0.025	0.031	0.041	0.060	0.091
NC	0.017	0.017	0.017	0.017	0.018	0.019	0.020	0.022	0.024	0.030	0.045
LQR-33V /LQR-2V	77%	86%	87%	84%	80%	74%	67%	63%	64%	67%	51%
LQR-33V /NC	56%	59%	64%	67%	68%	68%	67%	68%	68%	65%	53%

References

[1] The Japan Society of Seismic Isolation. Recent Trends in Seismic Isolation Buildings, http://www.jssi.or.jp/menshin/doc/keizoku2.pdf (in Japanese).

[2] Spencer Jr B. F., Nagarajaiah S. State of the Art of Structural control, ASCE Structural Engineering 2007; 129: 845–856.

[3] Loh C., Lin P., Chung N. Experimental verification of building control using active bracing system. Earthquake engineering and structural dynamics 1999; 28: 1099–1119.

[4] Miyamoto K., She J., Imani J., Xin X., Sato D. Equivalent-input-disturbance approach to active

structural control for seismically excited buildings. Eng Struct 2016; 125: 392–399.

[5] She J., Sekiya K., Wu M., Lei Q. Active structural control with input dead zone based on equivalent-input-disturbance approach. In: Proc of 36th annual conference on IEEE industrial electronics society 2010; 47–52.

[6] Aldemir U., Yanik A., Mehmet B. Control of structural response under earthquake excitation. Computer-Aid Civil Infrastruct Eng 2012; 27: 620–38.

[7] Park K., Ok S.: Optimal design of actively controlled adjacent structures for balancing the mutually conflicting objectives in design preference aspects. Eng Struct 2012; 45: 213–222.

[8] Fitzgerald B., Basu B.: Structural control of wind turbines with soil structure interaction included. Eng Struct 2016; 222: 131–151.

[9] Fallah A., Ebrahimnejad M. Active control of building structures using piezoelectric actuators. Applied Soft Computing 2013; 13: 449–461.

[10] Shi Y., Becker T. C., Furukawa S., Sato E., Nakashima M. LQR control with frequency-dependent scheduled gain for a semi-active floor isolation system. Earthquake engineering and structural dynamics 2014; 43: 1256–1284.

[11] Amini F., Ghaderi P. Seismic motion control of structures: A developed adaptive backstepping approach. Computers and Structures 2013; 114–115; 18–25.

[12] Park K., Ok S. Hybrid control approach for seismic coupling of two similar adjacent structures. Journal of Sound and Vibration 2015; 349: 1–17.

[13] Kim D.: Neuro-control of fixed offshore structures under earthquake 2009; 31: 517–522.

[14] Sadek F., Mohraz B. Semiactive control algorithms for structures with variable dampers. Journal of Engineering Mechanics 1998; 134: 981–990.

[15] Etedali, Sadegh, and Tavakoli Saeed. PD/PID Controller Design for Seismic Control of High-Rise Buildings Using Multi-Objective Optimization: A Comparative Study with LQR Controller. Journal of Earthquake and Tsunami; 2017; 11(3).

[16] Shih Yu C., Shih Wei Y., Lyan Ywan L., and Chih Hua P. Experimental verification of leverage-type stiffness-controllable tuned mass damper using direct output feedback LQR control with time-delay compensation. EARTHQUAKES AND STRUCTURES. 2017; 12(4): 425-436.

[17] Preumont A., Seto A. Active Control of Structures. WILEY. 2008.

[18] Fujii T., Fujitani H., Mukai Y. Performance evaluation of semiactive optimal control system by MR damper, J. Struct. Constr. Eng. 2013; 689: 1237–1245.

[19] C. A. Harvey and G. Stein. Quadratic Weights for Asymptotic Regulator Properties. IEEE Transaction Automatic Control, 1978; 23(3): 378–388.

[20] Elumalai, Vinodh Kumar and Subramanian, Raaja Ganapathy. A new algebraic LQR weight selection algorithm for tracking control of 2 DoF torsion system. ARCHIVES OF ELECTRICAL ENGINEERING. 2017; 66(1): 55–75.

[21] Naoya K. and Etsujiro S. A Method of Deciding Weighting Matrices in an LQ-Problem to Locate All Poles in the Specified Region. IFAC Proceeding Volumes, 1981; 14(2): 481–486.

[22] Takao F., Sadaaki K., and Osamu K. Synthesis of ILQ control system for disturbance attenuation. Proceeding of SICE Annual Conference. 2008; 1300–1303.

[23] Mockus J. On Bayesian methods for seeking the extremum, In Proc. IFIP Technical Conference 1974: 400–404.

[24] Roberto C., André S., Jan P., Marc P. D. Bayesian optimization for learning gaits under uncertainty. Annals of Mathematics and Artificial intelligence 2016; 76: 5–23.

[25] Alonso M., Philipp H., Heannette B., Stefan S., Sebastian T. Automatic LQR tuning based on gaussian process global optimization. 2016 IEEE international conference on robotics and automation (ICRA) 2016.

[26] Trimpe S., Millane A., Doessegger S., D' Andrea R. A self-tuning LQR approach demonstrated on an inverted pendulum. The international federation of automatic control 2014; 11281–11287.

[27] Sato D., Kasai K., Tamura T. Influence of frequency sensitivity of viscoelastic damper on wind-induced response. J Struct Constr Eng 2009; 635: 75–82 (in Japanese).

[28] Yanik A., Aldemir U., and Bakioglu M. Seismic vibration control of three dimensional structures with a simple approach. Journal of vibration engineering & technologies. 2016, 4(3): 235–247.

[29] Aldemir U., Bakioglu M., and Akhiev S. S. Optimal control of linear buildings under seismic excitations. Earthquake engineering and structural dynamics. 2001; 30: 835–851.

[30] Yanik A., Aldemir U. and Bakioglu M. A new active control performance index for vibration control of three-dimensional structures. Engineering Structrues. 2014; 62-63: 53–64.

[31] Kou M., Daiki S., and Jinhua S. A new performance index of LQR for combination of passive base isolation and active structural control. Engineering Structures. 2018; 157(15): 280–299.

[32] Tanaka Y., Fukuwa N., Tobita J., Mori M. Development and analysis of database for base-isolated buildings in Japanese. J. Technolo 2011; 17: 79–84.